

Photocatalytic process augmented with micro/nano bubble aeration for enhanced degradation of synthetic dyes in wastewater

Orawan Rojviroon, Thammasak Rojviroon*

Division of Environmental Engineering, Faculty of Engineering, Rajamangala University of Technology Thanyaburi, Pathum Thani, 12110, Thailand



ARTICLE INFO

Keywords:

Dissolved oxygen
Indigo carmine
Langmuir-Hinshelwood
Photooxidation
Reactive black 5

ABSTRACT

This research combines TiO_2 nanopowder photocatalyst (TNP) with micro/nano bubble aeration (MNBA) to enhance the dye degradation of the photocatalytic process treating synthetic dye wastewater. The experimental synthetic dyes were indigo carmine (IC) and reactive black 5 (RB5). The dye degradation performance of the photocatalytic process without MNBA (TNP + UVA) and with MNBA (TNP + UVA + MNBA) under various initial dye concentrations were evaluated. The results showed that, given the initial IC and RB5 dye concentrations of 2 μM , the degradation efficiency of TNP + UVA and TNP + UVA + MNBA were 100%. With higher dye concentrations (4–10 μM), the degradation efficiency of TNP + UVA and TNP + UVA + MNBA were between 84.05–98.20% and 90.64–100%. The kinetics of the photodegradation reaction of both dyes were described by the Langmuir-Hinshelwood kinetic model. The pseudo first order degradation rate constants of the photocatalytic process with MNBA were 1.44 and 1.66 times higher than those without MNBA for IC and RB5.

1. Introduction

During the recent decades, considerable attempts have been made to improve the pollutant degradation performance of advanced oxidation processes (AOPs). The aim is to reduce the investment outlay and operating costs of the wastewater treatment system while still effectively treating the influent containing highly toxic substances and complex-structure compounds [1,2].

Evidence shows that higher oxygen concentrations enhance oxidation reaction in the wastewater treatment system [3–5]. Specifically, micro/nano bubble aeration (MNBA) is a technique to deliver oxygen into the wastewater treatment system in order to increase the dissolved oxygen (DO) levels in the system. The increased DO levels enhance the oxidation reaction and subsequently wastewater treatment efficiency.

Unlike in the conventional fine bubble-aerated system, the aqueous system aerated with micro/nano-sized bubbles (MNB) is supersaturated with dissolved oxygen (DO) [6,7]. The advantages of MNB over the conventional system include higher DO stability, larger surface volume ratio, and higher mass transfer efficiency [5]. Besides, the MNBA-generated ultra-fine bubbles could remain in the aqueous system for hours or days (i.e., longer service time), subsequently promoting the proliferation of reactive oxygen species (ROSS), including singlet oxygen (1O_2), hydrogen peroxide (H_2O_2), hydroxyl radicals ($\bullet OH$), and superoxide radicals ($\bullet O_2^-$) [8,9]. The MNBA technology is adopted in various applications, such as cleaning and descaling solid surfaces, degrading organic pollutants, removing micropollutants, disinfecting water, and improving photocatalytic degradation of organic contaminants [10–13].

* Corresponding author.

E-mail address: thammasak@rmutt.ac.th (T. Rojviroon).



Fig. 1. High voltage plasma RMUTT-MNB generator.

Highly colored wastewater from the textile dyeing industry contains dyes of large molecular size and complex structure, making it highly biodegradation-resistant. Besides, the dye wastewater is highly toxic and can contaminate natural waterways if improperly treated [14–16]. As a result, several attempts have been made to improve the oxidation capability of AOPs.

The AOPs, including the photocatalytic process, are shown to be effective in degrading pollutants of various groups [17–19]. The degradation effectiveness is nevertheless dependent upon the oxygen mass transfer rate which influences the extent to which the photodegradation reaction proceeds and the types of final products, especially when reacting with highly complex-structure and/or highly degradation-resistant compounds [20]. As a result, the combination of MNBA with AOP, specifically the photocatalytic process, is expected to enhance the degradation efficiency of the wastewater treatment system.

Specifically, this research proposes a technique that combines TiO₂ nanopowder photocatalyst (TNP) with MNBA to enhance the dye degradation of the photocatalytic process. The experimental synthetic dyes included indigo carmine (IC) and reactive black 5 (RB5), and the initial dye concentrations were varied between 2, 4, 6, 8, and 10 µM. The dye degradation performance of the photocatalytic process without MNBA (TNP + UVA) and with MNBA (TNP + UVA + MNBA) were compared. The changes in the molecular structure of degraded dyes into various intermediate products were monitored throughout the experiment. Besides, the Langmuir-Hinshelwood (LH) kinetics of the heterogeneous reaction mechanisms of TNP and MNBA were also investigated. The novelty of this research lies in the use of MNBA, in combination with TNP and UVA, to effectively enhance the dye degradation performance of the photocatalytic oxidation process.

2. Experimental setup

2.1. Materials

In this research, TNP was purchased from US Research Nanomaterials, Inc. (Code US3490). MNBA was generated by the high voltage plasma RMUTT-MNB generator (12 kVp), a locally-made machine with the maximum water flow rate of 0.1 L min⁻¹ and pressure of 200–270 kPa (Fig. 1).

2.2. Characterization of TNP and MNBA

The morphology and particle size of TNP were determined by transmission electron microscopy (TEM, JEM-1400 TEM instrument), and the elemental composition analysis was carried out by an X-ray fluorescence spectrometer (XRF, Bruker model S8 Tiger). The pore size distribution and Brunauer-Emmett-Teller (BET) surface area were obtained from nitrogen adsorption-desorption isotherms by the BET instrument (BELSORPmax Bel Japan Inc.). Meanwhile, the particle size, size distribution and concentration of MNBA in the aqueous system was measured by NanoSight NS300 (Malvern Panalytical, Japan). The average DO concentration in the aqueous system was measured by a dissolved oxygen meter (DO 110 hand-held, EUTECH Instruments).

2.3. Photocatalytic degradation of dye

The enhanced degradation performance of the photocatalytic process with MNBA (TNP + MNBA with UVA irradiation) was measured by dye decolorization and gradation into intermediate products in batch reactor. A 2,000 mL beaker was used as the photoreactor (reaction chamber) irradiated with UVA light, given the average light intensity of 1,580 µW cm⁻² (Fig. 2). A UV light meter (UV-340; Lutron Electronic Enterprise Co., Ltd.) was used to measure the average light intensity.

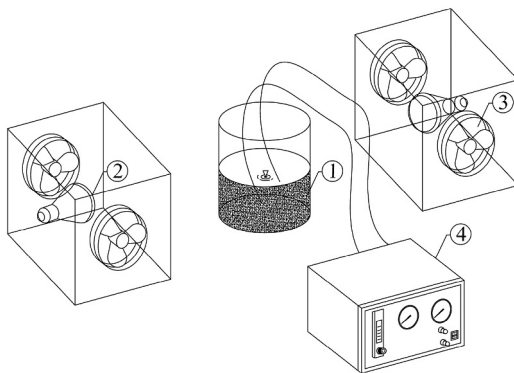


Fig. 2. Schematic of the photoreactor for synthetic dye degradation.

Table 1

The experimental conditions of this research given the dye concentrations of 2, 4, 6, 8, and 10 μM .

Experimental condition	TNP	UVA	MNBA
1	✓	✓	✓
2	✓	✓	-
3	✓	-	✓
4	-	✓	✓
5	-	✓	-
6	-	-	✓
7	✓	-	-

Note: ✓ indicates the use of the material and/or method.

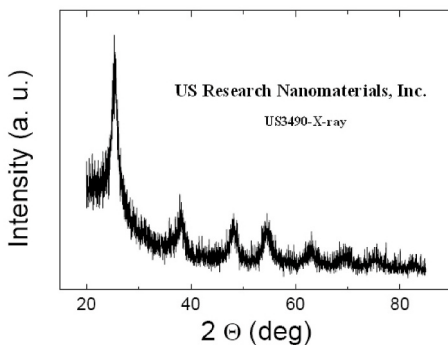


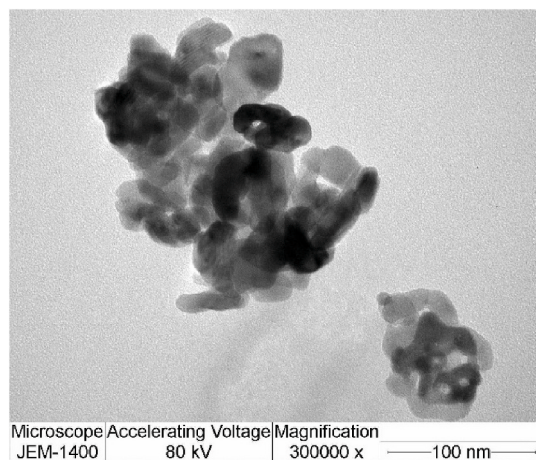
Fig. 3. The XRD image of TNP (Source: <https://www.us-nano.com/inc/sdetail/269>).

The IC and RB5 synthetic dye wastewater were separately prepared, and the initial dye concentrations were varied between 2, 4, 6, 8, and 10 μM . The photoreactor was independently filled with 1,000 mL of IC and RB5 synthetic dye wastewater before applying 0.1 g TNP and MNBA of 0.1 L min^{-1} flow rate. Prior to the experiment, samples were taken for measurement of initial dye concentrations before exposure to the UVA light.

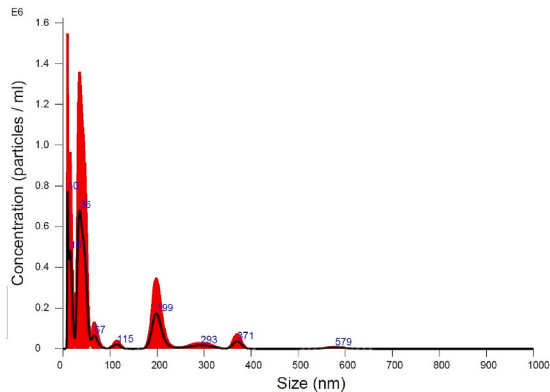
The dye concentrations were periodically measured throughout the 90-min experiment. Due to the water loss through evaporation of approximately 5% of the total volume of water in the photoreactor, the evaporated water was compensated by adding an equal amount of water to the photoreactor before the collection of samples.

The dye concentrations were analyzed by a spectrophotometer (Libra S12 visible and UV) and the toxic intermediate products by a gas chromatograph-mass spectrometer (GC-MS; model GC 6890 N Agilent) with Agilent G1888 headspace sampler as the injection source, Agilent HP-5ms as the capillary column, and MSD 5973 N Ionsource EI Single Quat as the detector.

To investigate the dye degradation enhancement of the photocatalytic process with MNBA (i.e., TNP + UVA + MNBA), this research compares the IC and RB5 dye degradation performance of the photocatalytic process with MNBA with those of the photocatalytic system without MNBA (TNP + UVA) under variable initial dye concentrations. The kinetics were subsequently determined based on the dye degradation performance of the photocatalytic process with and without MNBA. **Table 1** tabulates the experimental conditions carried out in this research, and there are seven experimental conditions.

**Fig. 4.** TEM image of TNP.**Table 2**
Composition and properties of TNP.

Catalyst	Particle size, nm	Composition, %		Pore volume, $\text{m}^3\cdot\text{g}^{-1}$	BET surface area, $\text{m}^2\cdot\text{g}^{-1}$
		TiO ₂	Other		
TNP	15–20	99.1	0.90	4.843×10^{-7}	1.298×10^2

**Fig. 5.** Particle size, size distribution, and concentration of MNB.

3. Results and discussions

3.1. TNP and MNBA characterization

The XRD results of TNP (Fig. 3) were from the website of the manufacturer of the nanoparticles (US Research Nanomaterials, Inc.) with the anatase crystalline phase of +99.5% and particle size of 10–25 nm.

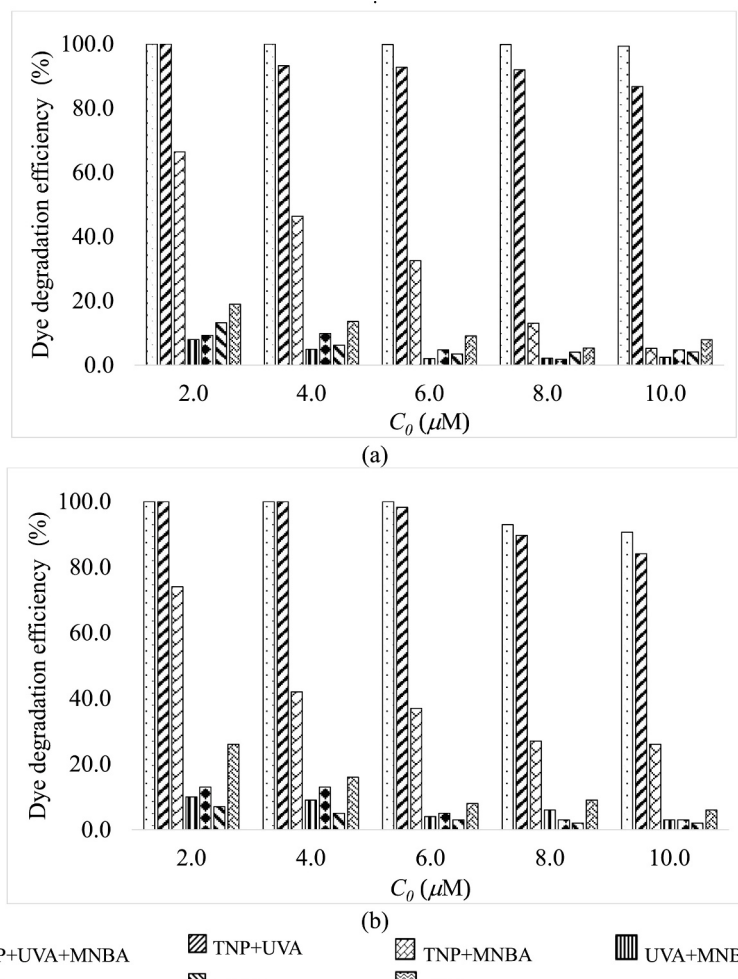
The TEM images indicate that the morphology of TNP is of high-quality lattice fringes without distortion (Fig. 4), with the average particle diameter of 15–20 nm. Table 2 tabulates the XRF and BET analysis results of TNP. The BET surface area of TNP was determined by the N₂ adsorption/desorption of TNP.

Fig. 5 shows the characteristics of MNB in the aqueous system. In this research, the MNBs were generated by circulating water in the RMUTT-MNB generator. As shown in Fig. 5, the majority of MNB bubbles were smaller than 100 nm, with the size distribution between 10 and 579 nm, the concentration in the aqueous system of 106 bubbles.mL⁻¹, and the average DO concentration of 25.8 mg L⁻¹.

Table 3

Dye degradation efficiency of TNP + UVA + MNBA and TNP + UVA at 90 min with different initial dye concentrations.

Dye type	Initial concentration [μM]	Degradation efficiency \pm SD (%) with n = 5	
		TNP + UVA + MNBA	TNP + UVA
IC	2	100.00 \pm 0.00	100.00 \pm 0.00
	4	100.00 \pm 0.00	93.22 \pm 0.33
	6	99.84 \pm 0.20	92.77 \pm 0.37
	8	99.80 \pm 0.24	91.96 \pm 0.20
	10	99.32 \pm 0.11	86.73 \pm 0.38
RB5	2	100.00 \pm 0.00	100.00 \pm 0.00
	4	100.00 \pm 0.00	95.00 \pm 0.02
	6	100.00 \pm 0.00	98.20 \pm 0.00
	8	92.96 \pm 0.19	89.69 \pm 0.24
	10	90.64 \pm 0.10	84.05 \pm 0.07

**Fig. 6.** Comparison of dye degradation efficiency under different experimental conditions and initial dye concentrations (C_0): (a) IC, (b) RB5.

3.2. Photocatalytic activity test

The dye degradation efficiency under experimental condition 1 (TNP + UVA + MNBA) at termination (i.e., after 90 min), given the initial dye concentrations of 2, 4, 6, 8, and 10 μM , were 99.32–100.00% and 92.96–100.00% for IC, and RB5, respectively. Under experimental condition 2 (TNP + UVA), the IC and RB5 dye degradation efficiency were 86.73–100.00% and 84.05–100.00%, respectively. Table 3 compares the IC and RB5 dye degradation performance under experimental condition 1 (TNP + UVA + MNBA) and 2 (TNP + UVA), and the results show that MNBA significantly increased the dye degradation performance of the photocatalytic

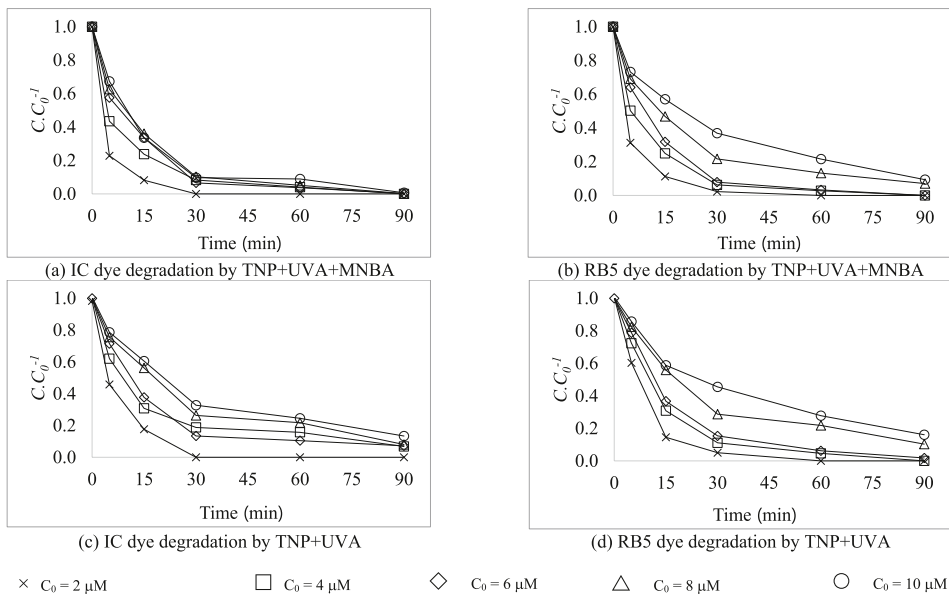


Fig. 7. Dye degradation by the photocatalytic process with MNBA (TNP + UVA + MNBA) and without MNBA (TNP + UVA).

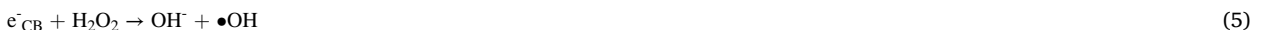
process, especially for wastewater containing high initial dye concentrations, as shown in Fig. 5.

Under experimental conditions 3 (TNP + MNBA without UVA irradiation) and 4 (UVA + MNBA without TNP), there was no photocatalytic activity due to the absence of photocatalyst (i.e., TNP) or UVA light source. The results showed that the dye adsorption of TNP were very low, with 18.97% and 26.00% for IC and RB5, respectively, at the initial concentration of 2 μM . Meanwhile, experimental conditions 5 (UVA), 6 (MNBA), and 7 (TNP) were operationally unsuitable for dye degradation due to low degradation efficiency (Fig. 5).

As shown in Table 3 and Fig. 6, with low initial dye concentrations, the IC and RB5 dye degradation efficiency of the photocatalytic process without MNBA (TNP + UVA) were operationally satisfactory. Essentially, the initial dye concentration (C_0) is the determinant of the dye degradation efficiency. Specifically, higher initial dye concentrations obscure the transmission of light energy onto the surface of the active site of photocatalyst [21,22]. Besides, higher dye concentrations reduce the generation of $\bullet\text{OH}$ and $\bullet\text{O}_2^-$ on the reactive catalyst surface [23–26].

The MNBA enhanced the dye degradation efficiency of the photocatalytic process (i.e., TNP + UVA + MNBA), especially for higher initial IC and RB5 dye concentrations. Besides, MNBA shortened the dye degradation time of the treatment system, as evidenced by the rapid degradation of IC and RB5 during the first 5 min through to 30 min (Fig. 7). The experimental results showed that MNBA significantly improve the dye degradation performance of the photocatalytic process (i.e., TNP + UVA + MNBA). The oxygen molecules on TNP act as electron acceptors to form $\bullet\text{O}_2^-$, which traps photoelectrons and reduces electron-hole recombination [13,27–29].

The MNBA enhanced the photocatalytic process whereby $\bullet\text{O}_2^-$ was first formed through the reduction reaction between e^-_{CB} and O_2 , as shown in Eq. (1). The intermediate product $\bullet\text{O}_2^-$ then undergoes a continuous chain reaction, as shown in Eqs. (2)–(5), resulting in the following ROSSs: $\bullet\text{O}_2^-$, H_2O_2 , and $\bullet\text{OH}$ [30–32].



where e^-_{CB} is the electron in the conduction band (CB) and $h\nu$ is the photon energy.

Under experimental condition 1 (TNP + UVA + MNBA), the micro- and nano-sized air bubbles (MNB) were constantly generated throughout the experiment. Besides, the size of MNB is positively correlated with the speed of MNB delivered into the system. The smaller MNB are more preferable as they can persist in the water for a much longer time, resulting in higher DO levels [33,34]. In addition, higher DO levels are also conducive to the formation and abundance of ROSSs, such as $^1\text{O}_2$, H_2O_2 , $\bullet\text{OH}$, and $\bullet\text{O}_2^-$. Specifically, the formation of the reactive free radicals is attributable to increasing DO levels in the photocatalytic degradation process [9,35,36].

The photocatalytic degradation process promoted oxidation, as evidenced by the rapid degradation of both dyes during the first

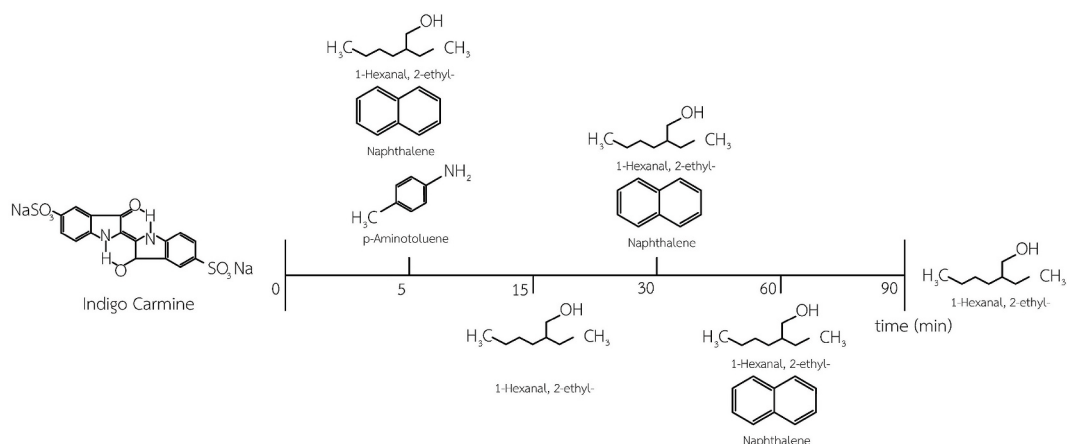


Fig. 8. Transformation of IC molecular structure during the photocatalytic process with MNBA (TNP + UVA + MNBA).

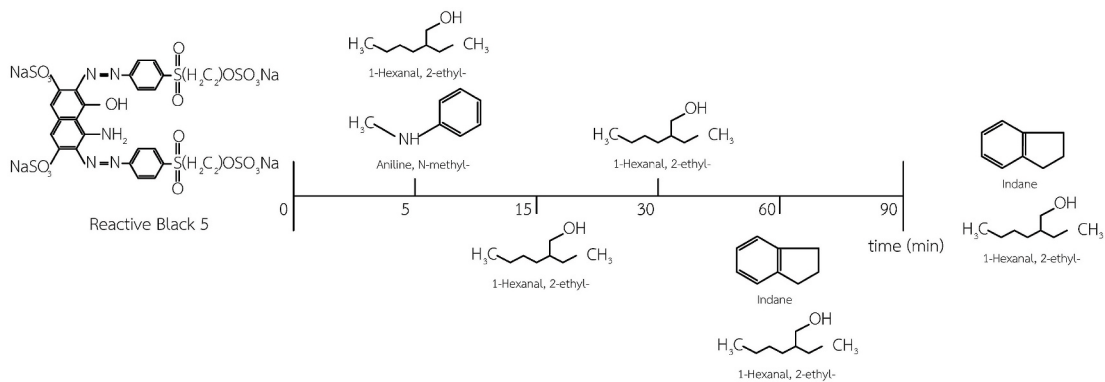


Fig. 9. Transformation of RB5 molecular structure during the photocatalytic process with MNBA (TNP + UVA).

5 min of the photocatalytic reaction. Afterward, the dye degradation rates gradually decreased as the incompletely degraded dyes in the form of dissolved organic matters (DOM) started to build up and accumulate on the surface of the photocatalyst [37,38].

The photocatalytic process is normally capable of oxidizing organic compounds to the most stable oxidation state and eventually to CO₂ and H₂O. In this research, although the reaction was incomplete, the transformation of dyes into simpler-structure by-products indicated that the ROSs under high DO conditions induced the cleavage mechanism for aromatic rings in the dye structure and destroyed the chromophore, causing the color to fade rapidly and the toxicity of the reaction products to decrease [39,40]. Figs. 8 and 9 show the complex structure and chromophore of IC and RB5 and their respective transformation during the photocatalytic degradation. The transformation patterns of IC and RB5 from GC-MS showed that the complex structure and chromophore of IC and RB5 were degraded into various products.

In [41–43], the photocatalytic process (without MNB) has been reported to break up the bonds at the junctions between fragile molecular structures or attack the bonds that are highly responsive to the ROSs, resulting in the intermediate products whose the molecular complexity remained relatively unchanged. The dye molecules were mainly attacked by hole in valence band (h⁺_{VB}) and ROSs in the photocatalytic process, inducing the oxidation of ring-opening reactions which resulted in the transformation of complex-structure products into less-complex-structure products [44,45]. In this current research, MNBA accelerated the dye degradation in the photocatalytic process, as evidenced by the rapid dye removal during the first 5 min of the experiment. Both the fragile and complex molecular structures, especially the aromatic ring structures, were destroyed, resulting in reduced molecular complexity and molecular size.

In addition, differences in the structure, complexity, and size of the molecules of both dyes also affected the degradation efficiency. RB5 has a larger molecular size and more complex chemical structure than IC, resulting in the former's lower degradation efficiency [18,46,47].

In this research, the Langmuir-Hinshelwood kinetic model (LH model) was used to describe the reaction mechanism of the photocatalytic process, which can be mathematically expressed as [48,49].

$$r_0 = \frac{kKC}{1+KC} \quad (7)$$

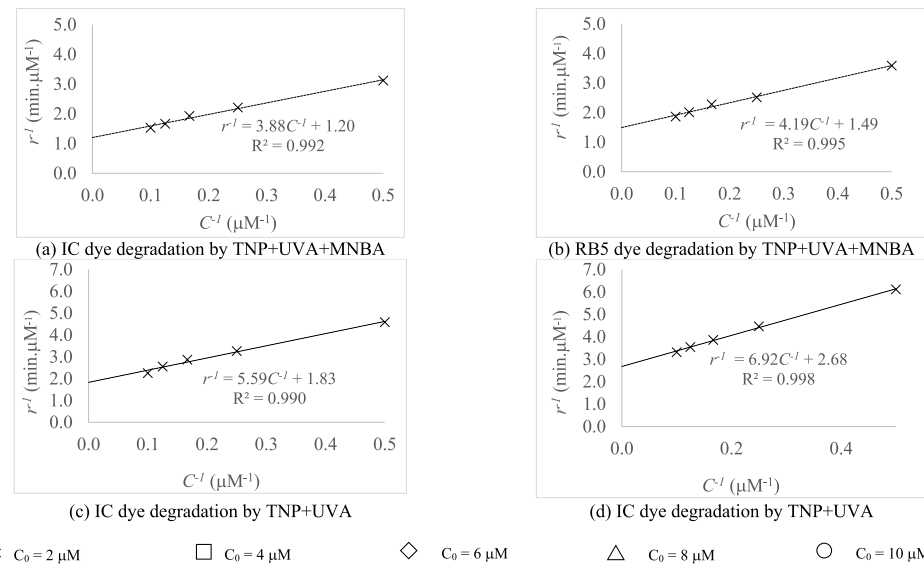


Fig. 10. LH kinetic plots of the dye degradation by the photocatalytic process with MNBA (TNP + UVA + MNBA) for (a) IC and (b) RB5 and by the photocatalytic process without MNBA (TNP + UVA) for (c) IC and (d) RB5.

Table 4

L-H kinetic parameters of the dye degradation of the photocatalytic process with and without MNBA.

Dye type	Experimental condition	k ($\mu\text{M} \cdot \text{min}^{-1}$)	K (μM^{-1})	kK (min^{-1})
IC	TNP + UVA + MNBA	0.833	0.309	0.257
	TNP + UVA	0.546	0.327	0.179
RB5	TNP + UVA + MNBA	0.671	0.356	0.239
	TNP + UVA	0.373	0.387	0.144

From Eq. (7), the mathematical expression can be further simplified into a linear equation in Eq. (8).

$$\frac{1}{r_0} = \frac{1}{kKC_0} + \frac{1}{k} \quad (8)$$

where r_0 is the initial photocatalytic degradation rate ($\mu\text{M} \cdot \text{min}^{-1}$), k is the apparent reaction rate constant ($\mu\text{M} \cdot \text{min}^{-1}$), K is the adsorption-to-desorption equilibrium rate constant (μM^{-1}), C_0 is the initial concentration of dye (μM), and C is the concentration of dye at any given experiment time (μM).

Fig. 10 illustrates the linear LH kinetic plots of the IC and RB5 dye degradation by the photocatalytic process without (TNP + UVA) and with MNBA (TNP + UVA + MNBA). The LH rate constant (k) and the Langmuir adsorption constant (K) of the dye degradation by the photocatalytic process with and without MNBA are tabulated in Table 4.

In terms of the pseudo first order reaction rate constants (kK), the photocatalytic degradation rate constants of the photocatalytic process with MNBA (TNP + UVA + MNBA) are about 1.44 and 1.66 times higher than those of the photocatalytic process without MNBA (TNP + UVA) for IC and RB5, respectively.

4. Conclusion

This experimental research combined MNBA with TNP to effectively enhance the IC and RB5 dye degradation performance of the photocatalytic process treating synthetic dye wastewater. The results showed that MNBA (i.e., TNP + UVA + MNBA) enhanced the dye degradation efficiency and dye degradation rates while shortening the operation time. In addition, MNBA increased the oxygen mass transfer rate in the system, subsequently lowering the molecular complexity and toxicity. Specifically, the MNBA could be integrated with the photocatalytic process to effectively enhance the dye degradation, especially in wastewater containing highly complex molecular substances of high concentrations.

Declaration of competing interest

The authors declare that they have no known competing financial interests or personal relationships that could have appeared to influence the work reported in this paper.

Acknowledgments

The authors would like to express heartfelt thanks to the Faculty of Engineering, Rajamangala University of Technology Thanyaburi (RMUTT). The authors are also grateful to the Thailand Research Fund (TRF): Area-based Collaborative Research (ABC) Grant “Development of fine bubble technology prototype with high voltage plasma for degradation of contaminants on vegetables” (Grant No. ABCRMUTT61B2-02) for the equipment support.

References

- [1] L. Bilińska, M. Gmurek, Novel trends in AOPs for textile wastewater treatment. Enhanced dye by-products removal by catalytic and synergistic actions, *Water Resour. For. Ind.* 26 (2021) 100160, <https://doi.org/10.1016/j.wri.2021.100160>.
- [2] Y. Hao, H. Ma, Q. Wang, L. Ge, Y. Yang, C. Zhu, Refractory DOM in industrial wastewater: formation and selective oxidation of AOPs, *Chem. Eng. J.* 406 (2021) 126857, <https://doi.org/10.1016/j.cej.2020.126857>.
- [3] Y.-Q. Hu, W. Wei, M. Gao, Y. Zhou, G.-X. Wang, Y. Zhang, Effect of pure oxygen aeration on extracellular polymeric substances (EPS) of activated sludge treating saline wastewater, *Process Saf. Environ. Protect.* 123 (2019) 344–350, <https://doi.org/10.1016/j.psep.2019.01.028>.
- [4] K. Abe, Y. Ozaki, Wastewater treatment by using kenaf in paddy soil and effect of dissolved oxygen concentration on efficiency, *Ecol. Eng.* 29 (2007) 125–132, <https://doi.org/10.1016/j.ecoleng.2006.02.003>.
- [5] J. Wu, K. Zhang, C. Cen, X. Wu, R. Mao, Y. Zheng, Role of bulk nanobubbles in removing organic pollutants in wastewater treatment, *Amb. Express* 11 (2021) 96, <https://doi.org/10.1186/s13568-021-01254-0>.
- [6] N. Matsuki, T. Ishikawa, S. Ichiba, N. Shiba, Y. Ujike, T. Yamaguchi, Oxygen supersaturated fluid using fine micro/nanobubbles, *Int. J. Nanomed.* 9 (2014) 4495–4505, <https://doi.org/10.2147/IJN.S68840>.
- [7] J.I. Lee, B.-S. Yim, J.-M. Kim, Effect of dissolved-gas concentration on bulk nanobubbles generation using ultrasonication, *Sci. Rep.* 10 (2020), <https://doi.org/10.1038/s41598-020-18816>.
- [8] L. Wang, J. Ali, Z. Wang, N.A. Oladoja, R. Cheng, C. Zhang, G. Mailhot, G. Pan, Oxygen nanobubbles enhanced photodegradation of oxytetracycline under visible light: synergistic effect and mechanism, *Chem. Eng. J.* 388 (2020) 124227, <https://doi.org/10.1016/j.cej.2020.124227>.
- [9] K. Yasui, T. Tuziuti, W. Kanematsu, Mysteries of bulk nanobubbles (ultrafine bubbles); stability and radical formation, *Ultrason. Sonochem.* 48 (2018) 259–266, <https://doi.org/10.1016/j.ulsonch.2018.05.038>.
- [10] A. Agarwal, W.J. Ng, Y. Liu, Principle and applications of microbubble and nanobubble technology for water treatment, *Chemosphere* 84 (2011) 1175–1180, <https://doi.org/10.1016/j.chemosphere.2011.05.054>.
- [11] W. Fan, et al., Bactericidal efficiency and photochemical mechanisms of micro/nano bubble-enhanced visible light photocatalytic water disinfection, *Water Res.* 203 (2021) 117531, <https://doi.org/10.1016/j.watres.2021.117531>.
- [12] W. Fan, W. An, M. Huo, D. Xiao, T. Lyu, J. Cui, An integrated approach using ozone nanobubble and cyclodextrin inclusion complexation to enhance the removal of micropollutants, *Water Res.* 196 (2021) 117039, <https://doi.org/10.1016/j.watres.2021.117039>.
- [13] W. Fan, Y. Li, C. Wang, Y. Duan, Y. Huo, B. Januszewski, M. Sun, M. Huo, M. Elimelech, Enhanced photocatalytic water decontamination by micro-nano bubbles: measurements and mechanisms, *Environ. Sci. Technol.* 55 (2021) 7025–7033, <https://doi.org/10.1021/acs.est.0c08787>.
- [14] T. Rojviroon, O. Rojviroon, S. Sirivithayapakorn, S. Angthong, V. Thongpool, Application of TiO₂ nanotubes as photocatalysts for decolorization of synthetic dye wastewater, *Water Resour. Ind.* (2021) 100163, <https://doi.org/10.1016/j.wri.2021.100163>.
- [15] M.R. Al-Mamun, S. Kader, M.S. Islam, M.Z.H. Khan, Photocatalytic activity improvement and application of UV-TiO₂ photocatalysis in textile wastewater treatment: a review, *J. Environ. Chem. Eng.* 7 (2019) 103248, <https://doi.org/10.1016/j.jece.2019.103248>.
- [16] M. Pirsahib, N. Moradi, A systematic review of the sonophotocatalytic process for the decolorization of dyes in aqueous solution: synergistic mechanisms, degradation pathways, and process optimization, *J. Water Proc. Eng.* 44 (2021) 102314, <https://doi.org/10.1016/j.jwpe.2021.102314>.
- [17] O. Rojviroon, T. Rojviroon, S. Sirivithayapakorn, Study of COD removal efficiency from synthetic wastewater by photocatalytic process, *Environ. Eng. Res.* 19 (2014) 255–259, <https://doi.org/10.4491/eer.2014.S1.002>.
- [18] T. Rojviroon, O. Rojviroon, S. Sirivithayapakorn, Photocatalytic decolourisation of dyes using TiO₂ thin film photocatalysts, *Surf. Eng.* 32 (2016) 562–569, <https://doi.org/10.1179/1743294415Y.0000000096>.
- [19] T. Rojviroon, S. Sirivithayapakorn, E. coli, Bacteriostatic action using TiO₂ photocatalytic reactions, *Int. J. Photoenergy* 2018 (2018) 8474017, <https://doi.org/10.1155/2018/8474017>.
- [20] T. Temesgen, T.T. Bui, M. Han, T.-i. Kim, H. Park, Micro and nanobubble technologies as a new horizon for water-treatment techniques: a review, *Adv. Colloid. Interfac.* 246 (2017) 40–51, <https://doi.org/10.1016/j.jcis.2017.06.011>.
- [21] P. Velusamy, G. Lakshmi, Enhanced photocatalytic performance of (ZnO/CeO₂) β -CD system for the effective decolorization of Rhodamine B under UV light irradiation, *Appl. Water Sci.* 7 (2017) 4025–4036, <https://doi.org/10.1007/s13201-017-0554-0>.
- [22] K.M. Reza, A.S.W. Kurny, F. Gulshan, Parameters affecting the photocatalytic degradation of dyes using TiO₂: a review, *Appl. Water Sci.* 7 (2017) 1569–1578, <https://doi.org/10.1007/s13201-015-0367-y>.
- [23] B. Fatima, S.I. Siddiqui, R. Ahmed, S.A. Chaudhry, Green synthesis of F-CdWO₄ for photocatalytic degradation and adsorptive removal of Bismarck Brown R dye from water, *Water Resour. For. Ind.* 22 (2019) 100119, <https://doi.org/10.1016/j.wri.2019.100119>.
- [24] M. Sadia, R. Naz, J. Khan, M. Zahoor, R. Ullah, R. Khan, S. Naz, H.S. Almoallim, S.A. Alharbi, Metal doped titania nanoparticles as efficient photocatalyst for dyes degradation, *J. King Saud Univ. Sci.* 33 (2021) 101312, <https://doi.org/10.1016/j.jksus.2020.101312>.
- [25] A. Ullah, et al., Mechanistic insight of dye degradation using TiO₂ anchored α -MnO₂ nanorods as promising sunlight driven photocatalyst, *Mater. Sci. Eng., B* 271 (2021) 115257, <https://doi.org/10.1016/j.mseb.2021.115257>.
- [26] K.T. Drisya, M. Solís-López, J.J. Ríos-Ramírez, J.C. Durán-Álvarez, A. Rousseau, S. Velumani, R. Asomoza, A. Kassiba, A. Jantrania, H. Castaneda, Electronic and optical competence of TiO₂/BiVO₄ nanocomposites in the photocatalytic processes, *Sci. Rep.* 10 (2020) 13507, <https://doi.org/10.1038/s41598-020-69032-9>.
- [27] W. Yu, J. Chen, M. Ateia, E.L. Cates, M.S. Johnson, Do gas nanobubbles enhance aqueous photocatalysis? experiment and analysis of mechanism, *Catalysts* 11 (2021), <https://doi.org/10.3390/catal11040511>.
- [28] G. Shen, X.H. Zhang, Y. Ming, L. Zhang, Y. Zhang, J. Hu, Photocatalytic induction of nanobubbles on TiO₂ surfaces, *J. Phys. Chem. C* 112 (2008) 4029–4032, <https://doi.org/10.1021/jp711850d>.
- [29] W. Fan, Z. Zhou, W. Wang, M. Huo, L. Zhang, S. Zhu, W. Yang, X. Wang, Environmentally friendly approach for advanced treatment of municipal secondary effluent by integration of micro-nano bubbles and photocatalysis, *J. Clean. Prod.* 237 (2019) 117828, <https://doi.org/10.1016/j.jclepro.2019.117828>.
- [30] A. Kondrakov, A. Ignatev, V.V. Lunin, F.H. Frimmel, S. Bräse, H. Horn, Roles of water and dissolved oxygen in photocatalytic generation of free OH radicals in aqueous TiO₂ suspensions: an isotope labeling study, *Appl. Catal. B Environ.* (2015), <https://doi.org/10.1016/j.apcatb.2015.09.038>.
- [31] J.d.M. Fonseca, M.J.d.S. Alves, L.S. Soares, R.d.F.P.M. Moreira, G.A. Valencia, A.R. Monteiro, A review on TiO₂-based photocatalytic systems applied in fruit postharvest: set-ups and perspectives, *Int. Food Res. J.* 144 (2021) 110378, <https://doi.org/10.1016/j.foodres.2021.110378>.
- [32] H. Dong, G. Zeng, L. Tang, C. Fan, C. Zhang, X. He, Y. He, An overview on limitations of TiO₂-based particles for photocatalytic degradation of organic pollutants and the corresponding countermeasures, *Water Res.* 79 (2015) 128–146, <https://doi.org/10.1016/j.watres.2015.04.038>.
- [33] A. Tekile, I. Kim, J.-Y. Lee, Extent and persistence of dissolved oxygen enhancement using nanobubbles, *Environ. Eng. Res.* 21 (2016) 427–435, <https://doi.org/10.4491/eer.2016.028>.
- [34] X. Bu, M. Alheshibri, The effect of ultrasound on bulk and surface nanobubbles: a review of the current status, *Ultrason. Sonochem.* 76 (2021) 105629, <https://doi.org/10.1016/j.ulsonch.2021.105629>.

- [35] J. Jin, R. Wang, J. Tang, L. Yang, Z. Feng, C. Xu, F. Yang, N. Gu, Dynamic tracking of bulk nanobubbles from microbubbles shrinkage to collapse, *Colloids Surf. A Physicochem. Eng. Asp.* 589 (2020) 124430, <https://doi.org/10.1016/j.colsurfa.2020.124430>.
- [36] T. Fujita, H. Kurokawa, Z. Han, Y. Zhou, H. Matsui, J. Ponou, G. Dodibiba, C. He, Y. Wei, Free radical degradation in aqueous solution by blowing hydrogen and carbon dioxide nanobubbles, *Sci. Rep.* 11 (2021) 3068, <https://doi.org/10.1038/s41598-021-82717-z>.
- [37] M. Maghsoudi, C. Jacquin, B. Teychené, M. Heran, V.V. Tarabara, G. Lesage, S.D. Snow, Emerging investigator series: photocatalysis for MBR effluent post-treatment: assessing the effects of effluent organic matter characteristics, *Environ. Sci. Water Res. Technol.* 5 (2019) 482–494, <https://doi.org/10.1039/C8EW00734A>.
- [38] Y. Ye, H. Bruning, X. Li, D. Yntema, H.H.M. Rijnaarts, Significant enhancement of micropollutant photocatalytic degradation using a TiO₂ nanotube array photoanode based photocatalytic fuel cell, *Chem. Eng. J.* 354 (2018) 553–562, <https://doi.org/10.1016/j.cej.2018.08.064>.
- [39] M.N. Chong, B. Jin, C.W.K. Chow, C. Saint, Recent developments in photocatalytic water treatment technology: a review, *Water Res.* 44 (2010) 2997–3027, <https://doi.org/10.1016/j.watres.2010.02.039>.
- [40] N. Montoya Sánchez, A. de Clerk, Autoxidation of aromatics, *Appl. Petrochem. Res.* 8 (2018) 55–78, <https://doi.org/10.1007/s13203-018-0199-4>.
- [41] M. Bilal, T. Rasheed, H.M.N. Iqbal, C. Li, H. Wang, H. Hu, W. Wang, X. Zhang, Photocatalytic degradation, toxicological assessment and degradation pathway of C.I. Reactive Blue 19 dye, *Chem. Eng. Res. Des.* 129 (2018) 384–390, <https://doi.org/10.1016/j.cherd.2017.11.040>.
- [42] R. Xie, K. Fang, Y. Liu, W. Chen, J. Fan, X. Wang, Y. Ren, Y. Song, Z-scheme In₂O₃/WO₃ heterogeneous photocatalysts with enhanced visible-light-driven photocatalytic activity toward degradation of organic dyes, *J. Mater. Sci.* 55 (2020) 11919–11937, <https://doi.org/10.1007/s10853-020-04863-5>.
- [43] S. Vigneshwaran, P. Sirajudheen, C.P. Nabeena, V.P. Sajna, S. Meenakshi, Photocatalytic performance of chitosan tethered magnetic Fe₂O₃-like (3D/2D) hybrid for the dynamic removal of anionic dyes: degradation and mechanistic pathways, *Int. J. Biol. Macromol.* 183 (2021) 2088–2099, <https://doi.org/10.1016/j.ijbiomac.2021.06.012>.
- [44] S. Verma, R.K. Dutta, Enhanced ROS generation by ZnO-ammonia modified graphene oxide nanocomposites for photocatalytic degradation of trypan blue dye and 4-nitrophenol, *J. Environ. Chem. Eng.* 5 (2017) 4776–4787, <https://doi.org/10.1016/j.jece.2017.08.026>.
- [45] A. Lebedev, F. Anariba, X. Li, D. Seng Hwee Leng, P. Wu, Ag/Ag₂O/BiNbO₄ structure for simultaneous photocatalytic degradation of mixed cationic and anionic dyes, *Sol. Energy* 178 (2019) 257–267, <https://doi.org/10.1016/j.solener.2018.12.040>.
- [46] A. Kumar, A review on the factors affecting the photocatalytic degradation of hazardous materials, *Mater. Sci. Eng. Int. J.* 1 (2017), <https://doi.org/10.15406/mseij.2017.01.00018>.
- [47] S. Natarajan, H.C. Bajaj, R.J. Tayade, Recent advances based on the synergistic effect of adsorption for removal of dyes from wastewater using photocatalytic process, *J. Environ. Sci.* 65 (2018) 201–222, <https://doi.org/10.1016/j.jes.2017.03.011>.
- [48] M.F. Atitar, A. Bouziani, R. Dillert, M. El Azzouzi, D.W. Bahnemann, Photocatalytic degradation of the herbicide imazapyr: do the initial degradation rates correlate with the adsorption kinetics and isotherms? *Catal. Sci. Technol.* 8 (2018) 985–995, <https://doi.org/10.1039/C7CY01903C>.
- [49] T. Wang, Y. Gao, T. Tang, H. Bian, Z. Zhang, J. Xu, H. Xiao, X. Chu, Preparation of ordered TiO₂ nanofibers/nanotubes by magnetic field assisted electrospinning and the study of their photocatalytic properties, *Ceram. Int.* 45 (2019) 14404–14410, <https://doi.org/10.1016/j.ceramint.2019.04.158>.